Low-Light-Level Optical Interactions with Rubidium Vapor in a Photonic Band-Gap Fiber

Saikat Ghosh, Amar R. Bhagwat, C. Kyle Renshaw, Shireen Goh, and Alexander L. Gaeta*
School of Applied and Engineering Physics, Cornell University, Ithaca, New York 14853, USA

Brian J. Kirby
Sibley School of Mechanical and Aerospace Engineering, Cornell University, Ithaca, New York 14853, USA
(Received 19 April 2006; published 13 July 2006)

We show that rubidium vapor can be produced within the core of a photonic band-gap fiber yielding an optical depth in excess of 2000. Our technique for producing the vapor is based on coating the inner walls of the fiber core with organosilane and using light-induced atomic desorption to release Rb atoms into the core. As an initial demonstration of the potential of this system for supporting ultralow-level nonlinear optical interactions, we perform electromagnetically induced transparency with control-field powers in the nanowatt regime, which represents more than a 1000-fold reduction from the power required for bulk, focused geometries.

DOI: 10.1103/PhysRevLett.97.023603 PACS numbers: 42.50.Gy, 32.80.Qk, 42.70.Qs

Remarkable advances have been made in the past decade in generating and controlling quantum states of light using atomic vapors [1–5]. In most cases, the underlying optical process for realizing these schemes has been the phenomenon of electromagnetically induced transparency (EIT) [6] in which a coherent superposition of atomic states is created by a strong control field such that an optically thick atomic ensemble is rendered transparent to a weak, resonant probe field. The concept of EIT has been applied and expanded to schemes that allow two extremely weak fields, which in principle can consist of single photon pulses, to strongly interact [7–10], which is critical for quantum network applications [5].

The two generic requirements to achieve EIT-based, ultralow-level optical interactions are (i) a large optical depth $\kappa = nL\sigma$, where n is the density of the atomic sample of length L and σ is the atomic absorption cross section, and (ii) confinement of the light beams to an area A comparable to the atomic scattering cross section of $3\lambda^2/2\pi$ [8–11]. For example, the phase shift due to nonlinear interactions between few photon pulses in the proposed scheme of [10] and the inverse of the critical power required to switch a signal field in the four-level scheme of [8] are each proportional to κ/A. In order to maximize the optical depth, a natural choice for the atomic ensemble is an alkali atom due to its relatively simple energy-level structure and its large σ as compared to, for example, molecules with rovibrational transitions [12]. There is a limit on how much κ can be increased by increasing the density n since this will result in undesirable dephasing effects due to atomic collisions. Alternatively, increasing the length L of the atomic sample can further enhance the optical depth. However, in a bulk focused geometry, this length L is limited to the Rayleigh length, which can be increased only by a corresponding increase in beam area A [5,10], and thus no change in the quantity κ/A.

In this Letter, we realize a new experimental geometry for alkali vapors that overcomes the limitations of bulk focused geometries by using light-induced atomic desorption (LIAD) to produce controllable densities of Rb atoms within a suitably coated core of a photonic band-gap fiber (PBGF). The photonic crystal structure [13] surrounding the core of a PBGF provides an unmatched ability to tightly confine light with a gas in a region a few microns in diameter over meter-long distances, and thus provides an ideal system to perform nonlinear optics at extremely low-light levels [10,11]. Recent demonstrations of nonlinear optical processes in PBGFs have used gases with relatively weak nonlinearities [12,14–16]. By using a gas such as alkali vapor with a strong nonlinear optical response, such a fiber system can form the basis for creation, manipulation, storage, and transmission of photonic states in a fiber geometry. However, until now, the ability to inject alkali atoms into PBGFs has eluded researchers due to the strong interaction of the vapor with silica walls of the fiber.

The primary challenge to creating a useful vapor of Rb atoms within a PBGF is that Rb vapor attacks and adheres to silica glass fiber walls through both physisorption, in which the atoms stick to the surface for a finite time, and chemisorption, in which the atoms are lost to the wall [17]. These issues are particularly severe for a fiber with a core 6 μm in diameter [18], which is a factor of 10^8 smaller than the atomic mean free path at room temperature. Furthermore, for the fraction of atoms undergoing physisorption, the spin decoherence is large [19], which makes this system unsuitable as a practical quantum device. However, treating a glass surface with paraffin or siloxane coatings [20] significantly alters the Rb-surface interaction properties such that the wall-induced dephasing rate decreases by 4 orders of magnitude with a significant reduction in chemisorption when compared with that for uncoated silica glass walls [21]. In addition, atoms attached to such coated walls can be released by sudden exposure to optical radiation through the nonthermal process termed LIAD [22–24].

We applied these techniques to the fiber geometry by surface modifying the core walls of a PBGF (AIR-6-800, crystal fiber, with a core diameter of 6 μm and a band gap extending from 750 to 810 nm, chosen to accommodate the D_1 and D_2 lines of Rb at 795 and 780 nm, respectively) with a monolayer of $C_{18}H_{35}$ moieties by self-assembly of octadecyldimethylmethoxysilane (ODMS) [25] via hydrolysis and condensation from solution. This monolayer deposition technique avoids the clogging of the fiber core that would occur for vacuum deposition of paraffin. The coating solution was introduced from polyolefin syringes to the PBGF via swaged fixtures, incubated in the core to facilitate the monolayer deposition, and then flushed out. The band gap of the fiber is preserved following the coating process. Following the monolayer deposition, the ends of the PBGF of length $L_{\text{fib}} = 25$ cm are placed in separate vacuum cells which are each connected to an ultrahigh vacuum system (Fig. 1). One of the cells (cell 1, in Fig. 1) is subsequently exposed to natural Rb vapor, at a pressure of 10^{-6} Torr, and a beam from an external-cavity diode laser reflected from a mirror inside the cell allows for monitoring the Rb density n_0 in the cell, which is kept at $n_0 = 2.1 \times 10^{10}$ cm^{-3}. Bulk condensation of Rb vapor inside the fiber core is prevented by maintaining a constant temperature along the entire length of the fiber. In the absence of LIAD, a finite fraction of atoms diffuse a length z down the fiber core of radius r_{fib}, and this atomic flux, which is proportional to the thermal velocity, can be estimated in the Knudsen limit [26]. A steady-state condition, known as ''ripening,'' is reached when this flux equals the rate of adsorption to the wall surface at z [24]. For the PBGF in which $L_{\text{fib}}/r_{\text{fib}} \simeq 10^5$, this ripening time can be extremely large. For simplicity, we rely on the Knudsen flow for the atoms to diffuse down the core. However, the atomic flux can be significantly enhanced with techniques such as light-induced drift [27] or dipole-force guidance [18] into the core. The total number of atoms in the core is

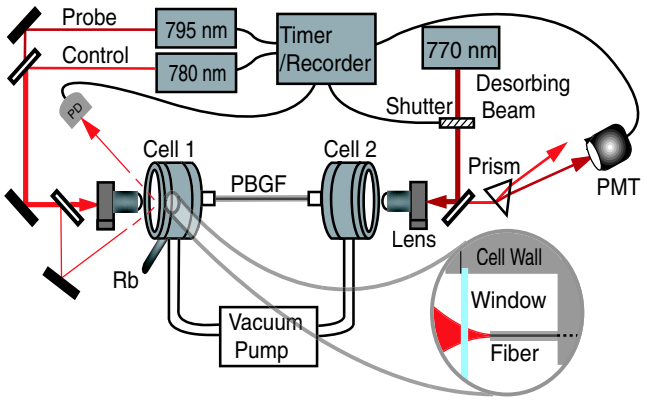

FIG. 1 (color online). A schematic of the experimental setup. Part of cell 1 is expanded to illustrate the region of the cell in front of the fiber tip. The beam reflected off a mirror at the back end of cell 1 is used to calibrate the density in the cell. PMT: photomultiplier tube.

determined by monitoring the transmission of a weak laser beam coupled to the core and by scanning over the D_1 transition. We take into account the density contribution due to the beam path in the cell before the fiber (Fig. 1) and fit the transmission coefficient,

$$T(\omega) = \exp\left\{-\int_0^{L_{\text{fib}}} n(z)dz \int_{-\infty}^{\infty} \sigma(v, \gamma, \omega) W(v) dv\right\}, \quad (1)$$

to the resulting absorption trace, where $n(z)$ is the atomic density at position z in the core and the absorption cross section σ of the transition is a function of the atomic velocity v, the homogeneous linewidth γ, and the laser frequency ω. The cross section is averaged over the Doppler profile $W(v)$. From the fit of Eq. (1) to the experimental trace, we estimate, in the absence of LIAD, the total number of atoms in the core to be $N_{\text{core}} = A_{\text{fib}} \int_0^{L_{\text{fib}}} n(z)dz \simeq 1.93 \times 10^3$, where A_{fib} is the cross-sectional area of the fiber core.

In our experiments, the intensity of the probe beam is maintained at 100 pW, which is an order of magnitude lower than the measured saturation power of 3 nW in the core. By coupling a desorbing beam counterpropagating to the probe beam into the core and tuned far off resonance at 770 nm, we observe a dramatic increase in the total number of atoms. Figure 2(a) shows that the atomic population undergoes a nearly instantaneous increase by 3 orders of magnitude after the turn-on of a 1-mW desorbing beam, with a maximum optical depth in excess of 2000. While a recent experiment [28] has reported Rb desorption from porous silica, we have not observed measurable desorption in uncoated fibers. From the fitted absorption profile, we estimate a homogeneous linewidth of $\gamma = 96$ MHz for the $F = 1 \rightarrow F' = 1, 2$ transitions. The broadening associated with the dipole dephasing of the atoms colliding with the core wall can be estimated from the wall-collisional frequency $\bar{v}/2r_{\text{fib}} \simeq 85$ MHz, where $\bar{v}$ is the thermal velocity, which suggests that the dominant contribution to the homogeneous linewidth is due to the wall-collisional dephasing as opposed to atomic collisional broadening. This is consistent with our data that show the linewidth to be nearly constant as a function of time as the density varies over 2 orders of magnitude.

As a result of the transient nature of the density of atoms within the core, application of this fiber system to low-light-level nonlinear optics requires a basic understanding of the dynamics of the desorbed atoms in order to determine the time window in which useful interactions can be performed. We apply the following simple model [23,24] to explain most of the features of the observed density dynamics. The temporal evolution of the total number N_{core} of atoms in the core is modeled by the equation

$$\frac{dN_{\text{core}}}{dt} = -\frac{\rho \bar{v} A_{\text{fib}}}{4} N_{\text{core}} + (\gamma_T + aI_d) N_{\text{wall}} + \xi(N_{\text{cell}} - N_{\text{core}}). \quad (2)$$

The first term on the right-hand side is the rate of loss of

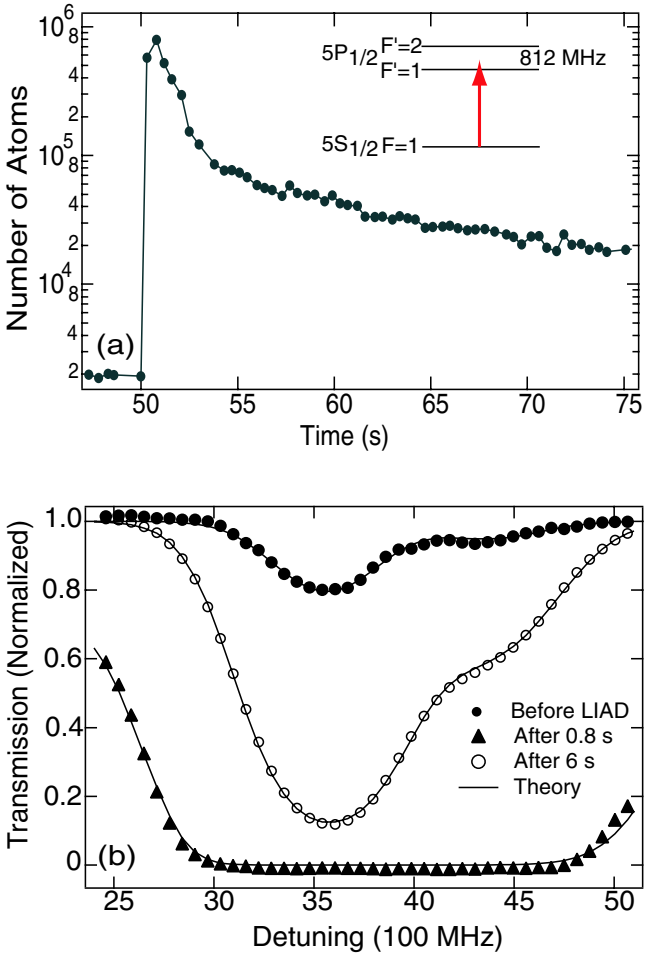

FIG. 2 (color online). (a) Measurement of the number of Rb atoms in the core of the photonic band-gap fiber as a function of time, obtained from a theoretical fit to the transition shown in the inset. (b) Variation of the absorption line shapes at three different times. The corresponding theoretically predicted absorption profile is shown by the solid line.

atoms from the core due to collisions with the walls, with the probability ρ that an atom sticks to the wall. The second term is the contribution from the N_{wall} atoms stuck to the core walls. This increase consists of two parts: a light-independent thermal desorption rate γ_T and a light-induced desorption rate, which is proportional to the intensity I_d of the desorbing beam at the core wall with a proportionality constant a. It is via this second process that the atomic density and the optical depth of the system can be varied. The last factor in Eq. (2) represents the relaxation of the atomic number to the steady-state value $N_{\text{cell}} = n_0 A_{\text{fib}} L_{\text{fib}}$ at a rate ξ. An equation similar to Eq. (2) is assumed for N_{wall}, where the first two factors contribute with opposite signs, leading to an increase and a decrease of atoms stuck to the walls, respectively. Figure 3 shows a plot of variation in the atomic population for various exposures of the desorbing beam of 60 μW, together with a fit of the adopted model.

To demonstrate the potential of this system to facilitate nonlinear optics at low-light levels, we investigate EIT in a V-type system with a probe at 100 pW and with control powers as low as 10 nW; these control powers are smaller by more than a factor of 1000 than what is typically used to achieve EIT in bulk geometries [29]. The probe is tuned to the $F = 2 \rightarrow F' = 1$ transition of the D_1 line of ^{87}Rb at 795 nm, and a control field, copropagating with the probe, is tuned to the $F = 2 \rightarrow F' = 3$ transition of the D_2 line at 780 nm. For this particular level scheme [inset of Fig. 4(b)], optical pumping between the hyperfine levels is avoided, since the $F = 1 \rightarrow F' = 3$ transition is dipole forbidden. Furthermore, the probe-field saturation and the optical pumping between the magnetic sublevels tend to cancel each other, and as a result the observed transparency is primarily due to pure EIT [29]. To analyze this system, we solve the density-matrix equations for a 3-level V system in steady state, with level a as the ground state and with b and c as the two excited states [Fig. 4(b)]. The coherence σ_{ca} to first order in the probe field is given by [12,30]

$$\sigma_{ca} = \frac{-i\Omega_p}{2[\gamma_{ac} - i\delta_p + \frac{|\Omega_c|^2/4}{\gamma_{bc}+i(\delta_c-\delta_p)}]}\Big\{(\rho^0_{cc} - \rho^0_{aa}) - \frac{|\Omega_c|^2(\rho^0_{bb} - \rho^0_{aa})}{4(\gamma_{bc} + i\delta_c)[\gamma_{bc} + i(\delta_c - \delta_p)]}\Big\}, \quad (3)$$

where Ω_c (Ω_p) and δ_c (δ_p) are the Rabi frequency and detuning, respectively, for the control (probe) field, ρ^0_{ii}, $(i = a, b, c)$ are the steady-state population distributions, $\gamma_{ij} = (\gamma_i + \gamma_j)/2 + \gamma^{\text{coll}}_{ij}$ $(i, j = a, b, c)$ are the dephasing rates, and γ_i is the decay rate of level i. The imaginary part of the Doppler-averaged susceptibility, calculated from this coherence, is integrated over the length of the fiber to fit to the transmission trace of the probe field.

Figure 4 show results in which a 1-mW desorbing beam releases Rb atoms into the core, and a series of probe transmission spectra are taken at ensuing time intervals.

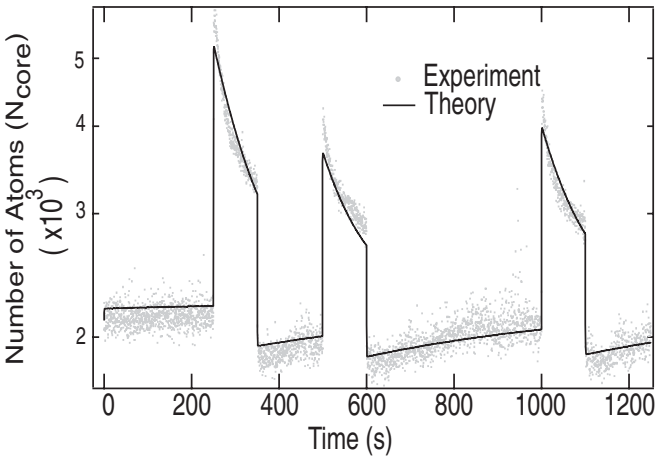

FIG. 3. Measurement of the number of Rb atoms in the core of the photonic band-gap fiber (dots) as a function of time in the presence of a 60 μW desorbing beam at 770 nm, with the theoretical fit (line) from Eq. (2) to the experiment.

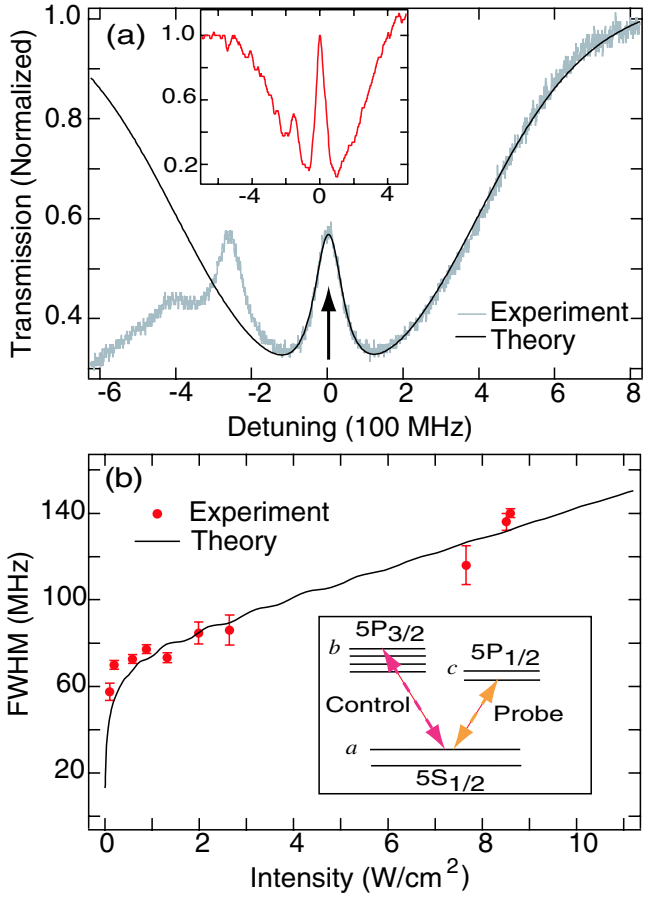

FIG. 4 (color online). (a) Transmission spectra of the probe field in the presence of a 361-nW control field. The arrow shows the transparency window due to EIT. The inset shows transparency larger than 90% for a probe scanned over $5S_{1/2}$, $F = 1 \rightarrow 5P_{1/2}$, $F' = 1$ with a 2.65 μW control field tuned to $5S_{1/2}$, $F = 1 \rightarrow 5P_{3/2}$, $F' = 1$ transition. (b) Experimental and theoretical variation of the EIT linewidth as a function of control intensity.

The time (250 ms) to obtain a trace is chosen to be long compared to the atomic time scales (hundreds of nanoseconds) but short compared to the time scales (seconds) associated with the desorption dynamics of the atomic density in the core. The input power of the probe field is set to 100 pW, and that of the control field is varied from 10 nW to 3 μW. Figure 4(a) shows a typical trace of the probe-field transmission in presence of a 361-nW control field, together with the corresponding theoretical fit as calculated from Eq. (3). Using the fitting procedure described in [12], we estimate a decay rate for the coherence between the two upper states to be $\gamma_{bc} = 24$ MHz and the two-level decoherence rates γ_{ai} $(i = b, c)$ to be between 90 and 100 MHz. Figure 4(b) shows the measured transparency full width at half maximum (FWHM) together with the corresponding FWHM calculated from Eq. (3). The error bar denotes the variation in measurements which were taken at different time intervals of atomic desorption [Fig. 2(a)]. At higher powers or for transitions in which optical pumping and saturation effects contribute, larger than 90% transparencies are observed [see inset of Fig. 4(a)].

In conclusion, we have demonstrated a new technique to create a significant density of rubidium vapor in the core of a PBGF, and as proof of the concept, we have demonstrated EIT in this system with a control power as low as 10 nW, which represents more than a factor of 10^7 reduction, as compared to acetylene-based systems in a PBGF [12,16].

We thank D. Gauthier, J. Hall, K. Koch, K. Moll, and J. Sharping for stimulating discussions, and D. Gauthier for the loan of the photomultiplier tube. We gratefully acknowledge support by the Center for Nanoscale Systems, supported by the NSF under Grant No. EEC-0117770, the Air Force Office of Scientific Research under Contract No. F49620-03-0223, and DARPA under the Slow-Light program.

*Electronic address: a.gaeta@cornell.edu

[1] A. Kuzmich *et al.*, Nature (London) **423**, 731 (2003).
[2] M. D. Lukin, Rev. Mod. Phys. **75**, 457 (2003).
[3] C. Liu *et al.*, Nature (London) **409**, 490 (2001).
[4] D. F. Phillips *et al.*, Phys. Rev. Lett. **86**, 783 (2001).
[5] L.-M. Duan *et al.*, Nature (London) **414**, 413 (2001).
[6] S. E. Harris, Phys. Rev. Lett. **62**, 1033 (1989).
[7] H. Schmidt and A. Imamoglu, Opt. Lett. **21**, 1936 (1996).
[8] S. E. Harris and Y. Yamamoto, Phys. Rev. Lett. **81**, 3611 (1998).
[9] S. E. Harris and L. V. Hau, Phys. Rev. Lett. **82**, 4611 (1999).
[10] A. André *et al.*, Phys. Rev. Lett. **94**, 063902 (2005).
[11] H. Schmidt and A. R. Hawkins, Appl. Phys. Lett. **86**, 032106 (2005).
[12] S. Ghosh *et al.*, Phys. Rev. Lett. **94**, 093902 (2005).
[13] R. F. Cregan *et al.*, Science **285**, 1537 (1999).
[14] F. Benabid *et al.*, Science **298**, 399 (2002).
[15] D. G. Ouzounov *et al.*, Science **301**, 1702 (2003).
[16] F. Benabid, P. Light, F. Couny, and P. Russell, Opt. Express **13**, 5694 (2005).
[17] J. H. de Boer, *Dynamical Character of Adsorption* (Oxford University Press, London, 1968).
[18] M. J. Renn *et al.*, Phys. Rev. Lett. **75**, 3253 (1995).
[19] W. Happer, Rev. Mod. Phys. **44**, 169 (1972).
[20] J. C. Camparo, J. Chem. Phys. **86**, 1533 (1987).
[21] M. A. Bouchiat and J. Brossel, Phys. Rev. **147**, 41 (1966).
[22] A. Gozzini *et al.*, Nuovo Cimento D **15**, 709 (1993).
[23] S. N. Atutov *et al.*, Phys. Rev. A **60**, 4693 (1999).
[24] E. B. Alexandrov *et al.*, Phys. Rev. A **66**, 042903 (2002).
[25] C. R. Kessel and S. Garnick, Langmuir **7**, 532 (1991).
[26] M. N. Kogan, *Rarefied Gas Dynamics* (Plenum Press, New York, 1969).
[27] H. G. C. Werij *et al.*, Phys. Rev. Lett. **52**, 2237 (1984).
[28] A. Burchinati *et al.*, Europhys. Lett. **67**, 983 (2004).
[29] D. J. Fulton *et al.*, Phys. Rev. A **52**, 2302 (1995).
[30] A. Javan *et al.*, Phys. Rev. A **66**, 013805 (2002).